ACS APPLIED MATERIALS & INTERFACES

Editors' Choice

www.acsami.org

Research Article

A Hydrogen-Bonded Organic Framework Equipped with a Molecular Nanovalve

Sara A. Ghazal, Sarah W. Tabbalat, Felipe Gándara, Ala'a Al-Ghourani, Samah M. Abusulieh, Mahmoud Abdellatief, Suhair Sunoqrot, and Kyle E. Cordova*

Cite This: https://doi.org/10.1021/acsami.4c01171

Read Online

ACCESS | Metrics & More | Article Recommendations | Supporting Information

ABSTRACT: The concept of a molecular nanovalve is applied to a synthesized biocompatible hydrogen-bonded organic framework (HOF), termed RSS-140, to load, trap, and subsequently release an antioxidant on command. Specifically, we exploit the pore windows of RSS-140 (i.e., β-CD cavities) to first load and trap the antioxidant, Trolox, within the internal pores of the HOF (Trolox⊂RSS-140) and, to prevent it from leaching, utilize supramolecular chemistry to complex azobenzene (Azo) with β-CD (Trolox⊂Azo@RSS-140). The molecular nanovalve is fully realized upon exposing Trolox⊂Azo@RSS-140 to UV light with a specific wavelength, which induces Azo isomerization, Azo decomplexation from β-CD, and subsequent release of Trolox from the pores of RSS-140. The biocompatibility and nontoxicity of Trolox⊂Azo@RSS-140, together with the absolute control over the nanovalve opening, were established to yield a system that safely and slowly releases Trolox for longer-lasting antioxidant efficacy. As the field of supramolecular chemistry is rich with similar systems and many such systems can be used as building blocks to construct HOFs or other extended framework materials, we envision the molecular nanovalve concept to be applied widely for controllably delivering molecular cargo for diverse applications.

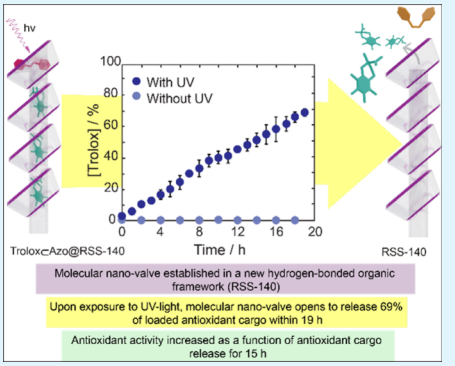

KEYWORDS: *hydrogen-bonded organic frameworks, molecular nanovalve, drug delivery system, targeted therapy, supramolecular chemistry*

INTRODUCTION

Configuring materials to predictably respond to an external stimulus (i.e., light, pH, temperature, chemical and/or biological environment, electric field, among others) for carrying out a specific function at the bulk level is the fundamental basis of molecular machinery.[1−5] Indeed, the chemistry of incorporating movable elements into biomolecular, molecular, supramolecular, and inorganic and/or hybrid inorganic−organic systems has been duly explored and developed in this regard, examples of which include mechanically interlocked molecules (e.g., catenanes, rotaxanes), pseudorotaxanes, porous inorganic materials (e.g., mesoporous silica), and metal−organic frameworks (MOFs).[6−17] The latter examples are of particular interest as control over access to and from the internal pore environments of porous inorganic materials and MOFs provides significant advantages for applications in molecular transport, chemical sensing, gas separation and storage, catalysis, and drug delivery.[18−22] Given that such systems are often endowed with accessible pore apertures, it appears obvious that installing a stimuli-responsive valve composed of movable elements is a critical step for controlling access of molecules to and from the internal pore environment.[23] Although mesoporous silica and MOFs have had "molecular nanovalves or valves" installed, noted examples are often overengineered with respect to extensive synthesis being required (i.e., tethering functional, movable molecules on the inorganic walls or organic building units) or remain at the mercy of the self-assembly and/or template-driven synthesis process.[8−15,24] Furthermore, often as a result of overengineering, facile control over the movable elements is relatively limited, thereby hindering overall performance.

Herein, we report the first fully organic porous extended framework whose pore apertures are of perfect size to not only encapsulate a biologically active antioxidant but also to install a molecular nanovalve to control diffusion of the antioxidant into and out of the internal pores. This hydrogen-bonded organic framework (HOF), termed RSS-140, was realized via a simple solvothermal reaction containing β-cyclodextrin (β-CD). Provided the widely known reversible and photocontrollable nature of azobenzene (Azo) and its ability to form supramolecular complexes with cyclodextrin,[25,26] we equip RSS-140 with an Azo-derived molecular nanovalve situated at the pore

Received: January 25, 2024
Revised: March 12, 2024
Accepted: March 14, 2024

apertures of this extended framework material to control the encapsulation and release of the biologically active antioxidant Trolox. It is noted that the structure of RSS-140 is analogous to several of the widely studied β-CD-based MOFs, thereby making the results of this study useful in providing other classes of materials with a straightforward approach to installing movable elements for achieving specific end functions. Finally, preliminary *in vitro* cellular studies (i.e., cytotoxicity and antioxidant ability) provide early indication of the safety and nontoxicity of Trolox⊂Azo@RSS-140 to human dermal fibroblast cells as well as its effectiveness in delivering on-demand antioxidant properties.

EXPERIMENTAL SECTION

Chemicals and Experimental/Analytical Techniques Used in This Work. Full details concerning the chemicals, materials, supplies, and experimental/analytical techniques used in this work are provided in the Supporting Information, Sections S1 and S2.

Single-Crystal X-Ray Diffraction Analysis. Single-crystal X-ray diffraction (SCXRD) was collected at the X-Ray Diffraction Facility of the Materials Science Institute of Madrid, with a Bruker D8 Venture diffractometer, using a microfocused source with Cu Kα radiation (λ = 1.54178 Å) operated at 50 kV and 1.2 mA, and a Photon III detector. Crystals were selected with an optical microscope, and diffraction data were collected over a hemisphere of the reciprocal space combining φ and ω scans, reaching a resolution of 0.85 Å, with a frame width of 0.5°, and exposure time adjusted based on the diffracting quality of each specimen. Data were reduced and scaled with APEX4 software, and the structures were solved by intrinsic phasing methods, using a SHELXT program. Structural refinement was carried out with the use of the OLEX2-1.5 and ShelXL programs. All nonhydrogen atoms were located and anisotropically refined. The position of part of the hydrogen atoms was identified in the difference Fourier maps, and for the rest of them, it was geometrically calculated and fixed, except for the Azo@β-CD complex, where there was a large amount of solvent water molecules present, for which the location of the H atoms could not be clearly assigned. Full data sets are available in the Cambridge Crystallographic Data Centre (CCDC; Nos. 2285699−2285701 for Trolox⊂RSS-140, RSS-140, and Trolox⊂Azo@RSS-140, respectively, and 2285816 for the Azo@β-CD complex).

Synchrotron-Radiation Powder X-Ray Diffraction Analysis. High-resolution synchrotron-radiation PXRD data (λ = 1.00098 Å) were collected using the MS beamline at SESAME. For each measurement, the sample was placed at a distance of 740.4 mm from a Pilatus 300 K area detector of 172 μm pixel size. The area detector covers 6.4° at 740.4 mm distance from the sample and was used to collect diffraction patterns from 1.3° to 43° with an average exposure time collected per detector frame of 240 s. Samples were packed in borosilicate glass capillaries and mounted on a standard goniometer head fixed to a capillary spinner. Data were collected in transmission mode (Debye−Scherrer geometry) at room temperature. A NIST (640f) Si standard was measured to calibrate the instrument, while the lattice parameter of Si was used to determine the exact wavelength during the measurements. The detector was set to collect a diffraction image every 6°, while the collected images were then processed to extract the merged diffraction pattern through an image J scripting mode. Pawley refinements for Trolox⊂RSS-140 and Trolox⊂Azo@RSS-140 samples using synchrotron powder diffraction data (λ = 1.00098 Å) were carried out using the Reflex module of Materials Studio software package, in the 2θ range = 2.2°−45°. Initial lattice parameters were taken from the single crystal data. A Pearson VII function was used to describe the pattern profile. Initial profile values were obtained from the refinement of the Si calibrant collected at the beamline. The background was refined with a 16-coefficient polynomial function, and the asymmetry correction was introduced with a three-parameter function. Final residual Rwp (without background) values of 2.57 and 8.68% were obtained for Trolox⊂RSS-140 and Trolox⊂Azo@RSS-140, respectively.

Complexation of Azobenzene with β-CD, Azo@β-CD Supramolecular Complex. The synthesis of the Azo@β-CD supramolecular complex was prepared by adding a solution of azobenzene (3.6 mg, 0.02 mmol) in MeOH (1.0 mL; 0.02 M) as a layer above a solution of β-CD (11 mg, 0.01 mmol) in water (5.0 mL; 0.002 M). The reaction was placed in a well-sealed glass vial and stored in the dark at room temperature for 14 d until orange cubic crystals appeared. The orange cubic crystals were collected by suction filtration and washed with toluene until no yellow color appeared in the filtrate. At this point, the solid was washed with cold water (3 × 2.5 mL). Yield = 77%. EA Calcd for $[(C_{42}H_{70}O_{35})_4(C_{12}H_{10}N_2)_4(CH_3OH)]\cdot 17H_2O$ = (β-CD)(Azo)-$(MeOH)_{0.25}\cdot 4.25H_2O$: C, 46.58; H, 6.36; N, 2.24%. Found: C, 46.52; H, 6.32; N, 2.23%.

Synthesis of RSS-140. In a Teflon-lined, stainless steel Parr autoclave (inner volume = 25 mL), β-CD (284 mg, 0.250 mmol) and KOH (56 mg, 1.00 mmol) were mixed in a 10 mL solution of water and MeOH (1:4 v:v, respectively). The poorly soluble mixture was stirred at room temperature for 1 h, at which point the autoclave was tightly capped and placed in an oven that was preheated at 140 °C (internal pressure was auto generated and not specifically monitored). After 3 d, the autoclave was removed from the isothermal oven and allowed to cool to room temperature. White crystals were collected by suction filtration and washed with MeOH (3 × 2.5 mL). Yield = 84%. ^{1}H NMR (500 MHz; DMSO-d_6): δ = 3.60 (m; 5 H), 4.44 (t; 1H), 4.82 (d; 1H), 5.67 (d; 1H), 5.71 ppm (d; 1H). EA Calcd C, 41.81; H, 6.52; N, 0.00%. Found: C, 41.80; H, 6.23; N, 0.00%.

Synthesis of Encapsulated Trolox in RSS-140, Trolox⊂RSS-140. In a Teflon-lined, stainless steel Parr autoclave (inner volume = 25 mL), β-CD (284 mg, 0.250 mmol), KOH (56 mg, 1.00 mmol), and Trolox (34 mg, 12% w/w of β-CD) were mixed in a 10 mL solution of water and MeOH (1:4 v:v, respectively). The poorly soluble mixture was stirred at room temperature for 1 h, at which time the autoclave was tightly capped and placed in an oven that was preheated at 140 °C (internal pressure was auto generated and not specifically monitored). After 3 days, the autoclave was removed from the isothermal oven and allowed to cool to room temperature. White crystals were collected by suction filtration without washing. Yield = 80%. Trolox loading = 1%. ^{1}H NMR (500 MHz; DMSO-d_6): δ = 3.60 (m; 5H), 4.45 (s; 1H), 4.81 (s; 1H), 5.75 (m; 2H), 8.30/8.43 (s; 1H). We note that both the 8.30 and 8.43 ppm chemical shifts are attributed to Trolox in different conformational arrangements within the pore. EA Calcd C, 39.30; H, 6.88; N, 0.00%. Found: C, 39.30; H, 6.52; N, 0.00%.

Synthesis of Encapsulated Trolox in Azobenzene-Capped RSS-140, Trolox⊂Azo@RSS-140. In a Teflon-lined, stainless steel Parr autoclave (inner volume = 25 mL), β-CD (284 mg, 0.250 mmol), KOH (56 mg, 1.00 mmol), and Trolox (34 mg, 12% w/w of β-CD) were mixed in a 10 mL solution of water and MeOH (1:4 v:v, respectively). The poorly soluble mixture was stirred at room temperature for 1 h, at which point azobenzene (36 mg, 0.20 mmol) was added before tightly capping the autoclave and placing the reaction mixture in an oven that was preheated at 140 °C (internal pressure was auto generated and not specifically monitored). After 3 d, the autoclave was removed from the isothermal oven and allowed to cool to room temperature. Yellow crystals were collected by suction filtration and washed with toluene until no yellow color appeared in the filtrate. Yield = 79%. Trolox loading = 1.65 ± 0.09%; azobenzene capping = 0.56 ± 0.05%. ^{1}H NMR (500 MHz; DMSO-d_6): δ = 3.60 (m; 5H), 4.45 (s; 1H), 4.81 (s; 1H), 5.76 (m; 2H), 7.14 (t; J = 7.5 Hz, 2H), 7.16 (d; J = 8.1 Hz, 4H), 7.24 (t; J = 7.5 Hz, 4H), 8.30/8.42 (s; 1H). We note that both the 8.30 and 8.42 ppm chemical shifts are attributed to Trolox in different conformational arrangements within the pore. EA Calcd C, 39.39; H, 6.87; N, 0.08%. Found: C, 39.38; H, 6.51; N, 0.07%.

Azo@β-CD Decomplexation. In a 5 mL quartz cuvette, the Azo@β-CD complex (1.0 mg) was mixed in cyclohexane (3 mL). The cuvette with the heterogeneous mixture was capped/closed with tape

https://doi.org/10.1021/acsami.4c01171
ACS Appl. Mater. Interfaces XXXX, XXX, XXX−XXX

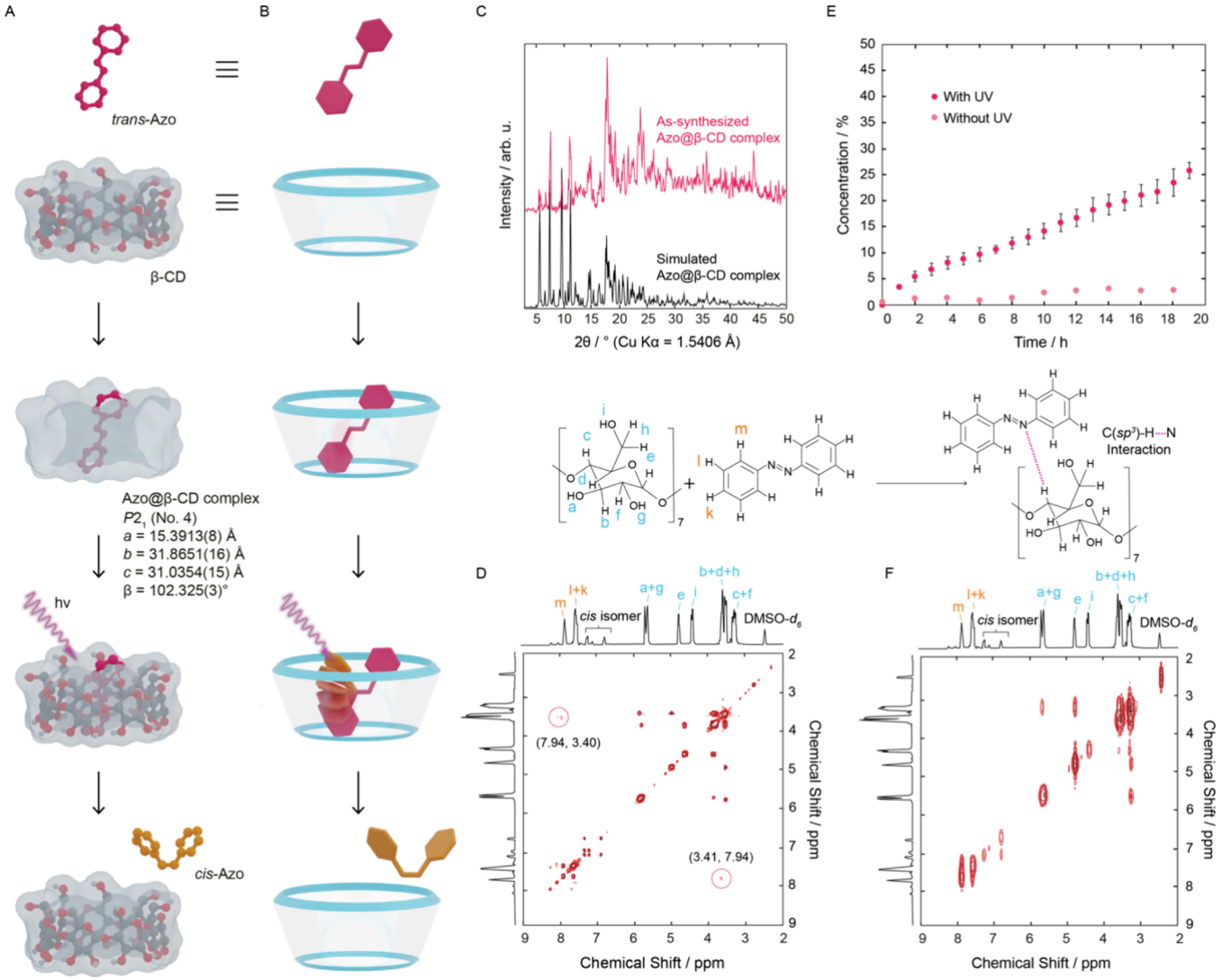

Figure 1. Synthesis, crystal structure, and structural characterization of the Azo@-β-CD supramolecular complex, which serves as the conceptual basis for a molecular nanovalve. (A) Reaction scheme for realizing the single crystal structure of the Azo@β-CD supramolecular complex, which upon irradiation with ultraviolet light (λ = 254 nm) leads to decomplexation upon photoisomerization of Azo. (B) Schematic illustration of the formation and deformation of the Azo@β-CD supramolecular complex. (C) Powder X-ray diffraction (PXRD) analysis of the as-synthesized Azo@β-CD supramolecular complex (pink) compared to the diffraction pattern simulated from the single crystal (black), demonstrating bulk phase purity. (D) ^{1}H−^{1}H homonuclear correlation nuclear magnetic resonance spectroscopy (^{1}H−^{1}H COSY NMR) for the as-synthesized Azo@β-CD supramolecular complex in deuterated dimethyl sulfoxide. (E) Concentration percentage of Azo in the supernatant after exposure to UV light and decomplexation from the Azo@β-CD supramolecular complex. Error bars represent the standard deviation based on results from three separate, independent trials. (F) ^{1}H−^{1}H COSY NMR for Azo@β-CD supramolecular complex after exposing the complex to UV light for 48 h. The characteristic chemical shifts associated with Azo@β-CD are absent, thereby demonstrating decomplexation. A synthetic scheme is provided above the ^{1}H−^{1}H COSY NMR spectra as a reference for relevant chemical shift assignments. Atom colors: C, gray; O, red; H, white.

and shaken to allow the crystals to completely settle to the bottom. The cuvette was then placed horizontally under a UV lamp to ensure equal exposure to UV light (254 nm) over 19 h. Starting a t = 0 h and continuing every hour for 19 h, the absorbance spectra were measured at λ = 320 nm (λ_{max} for *trans*-azobenzene).

Trolox Release from Trolox⊂RSS-140. In a 5 mL quartz cuvette, Trolox⊂RSS-140 (30.0 mg) was mixed with cyclohexane (3 mL). The cuvette with the heterogeneous mixture was capped/closed with tape and shaken to let the crystals completely settle to the bottom. Starting at t = 0 h and continuing every hour for 19 h, the absorbance spectra were measured at λ = 290 nm (λ_{max} for Trolox).

Nanovalve Opening and Trolox Release from Trolox⊂Azo@RSS-140. In a 5 mL quartz cuvette, Trolox⊂Azo@RSS-140 (30.0 mg) was mixed with cyclohexane (3 mL). The cuvette with the heterogeneous mixture was capped/closed with tape and shaken to let the crystals completely settle to the bottom. The cuvette was then placed horizontally under a UV lamp to ensure equal exposure to UV light (254 nm) over 19 h. Starting a t = 0 h and continuing every hour for 19 h, the absorbance spectra were measured at λ = 290 and 320 nm (λ_{max} for Trolox and *trans*-azobenzene, respectively). A separate experiment was carried out, in which Trolox⊂Azo@RSS-140 was exposed to UV light (254 nm) for 6 d with the absorbance spectra being measured once per day at λ = 290 and 320 nm (λ_{max} for Trolox and *trans*-azobenzene, respectively) until reaching full nanovalve opening and Trolox release.

Controlled Nanovalve Opening and Trolox Release in Trolox⊂Azo@RSS-140. In a 5 mL quartz cuvette, Trolox⊂Azo@RSS-140 (30.0 mg) was mixed in cyclohexane (3 mL). The cuvette with the heterogeneous mixture was capped/closed with tape and shaken to let the crystals completely settle to the bottom. The cuvette was then placed horizontally under a UV lamp to ensure equal exposure to UV light (254 nm). To demonstrate the controlled

https://doi.org/10.1021/acsami.4c01171
ACS Appl. Mater. Interfaces XXXX, XXX, XXX−XXX

opening of the Azo nanovalve in TroloxCAzo@RSS-140, the cuvette was exposed to UV light for 1 h and then the UV light was turned off for 2 h. Starting a t = 0 h and after any on and off UV light, the absorbance spectra were measured at λ = 290 and 320 nm (λ_{max} for Trolox and *trans*-azobenzene, respectively).

Cell Cultures. Biocompatibility and cytotoxicity were stablished using human dermal fibroblasts (HDFs). HDF cells were subcultured and grown in Dulbecco's Modified Eagle Medium (DMEM) at 37 °C in a 5% CO_2 incubator for 2 w. The HDF cells were supplemented with 10% heat-inactivated fetal bovine serum (FBS) and 1% penicillin−streptomycin antibiotics (100 μg mL^{-1}).

Cell Viability Assay. The HDF cells were detached from a confluent T-75 cm^2 culture flask at 2−8 passages using trypsin-EDTA solution. HDF cells were then seeded into 96-well plates at a density of 5000 cells well^{-1} and allowed to adhere for 24 h. After the time elapsed, the HDF cells (n = 5) were treated in the culture media with β-CD (control), Trolox (control), azobenzene (control), Azo@β-CD supramolecular complex (control), RSS-140 (control), TroloxCRSS-140 (control), and TroloxCAzo@RSS-140 (sample) with concentrations of 0, 0.1, 1, 10, 100, and 1000 μg mL^{-1} each for 72 h at 37 °C in a 5% CO_2 incubator. After the end of the incubation period, a resazurin assay was performed. Specifically, the culture media were removed for each treatment and replaced with 100 μL of fresh DMEM containing 10% v/v resazurin solution and incubated for an additional 2 h. During this 2 h incubation period, the resazurin blue dye is reduced by viable cells to highly fluorescent resorufin. Accordingly, the fluorescence of the well plates was read at 540/620 nm excitation/emission wavelengths using a multimode microplate reader. The HDF cell viability was then expressed as a percent relative to that of untreated cells. All assays were performed five times total each.

***In Vitro* Antioxidant Assays.** The antioxidant activity was determined by using a 2,2-diphenyl-1-picrylhydrazyl (DPPH) radical scavenging assay. For the assay, different concentrations (40, 80, and 160 mg mL^{-1}) of Azo@β-CD supramolecular complex (control) and RSS-140 (control) were prepared in DMSO. Then, 4 mL of 0.1 mM DPPH solution in ethanol was added to 200 μL of each sample, while for TroloxCAzo@RSS-140 (sample), 300 mg was mixed in cyclohexane (3 mL) in a 5 mL quartz cuvette. The cuvette with the heterogeneous mixture was capped/closed with tape and shaken to let the crystals completely settle to the bottom. Starting at t = 0 h and continuing every 5 h for 15 h, the sample was filtrated, and the filtrate was collected and evaporated to have Trolox and Azo only for dissolving in 200 μL of DMSO. Then, 4 mL of 0.1 mM DPPH solution in ethanol was added to each sample. Samples were mixed, incubated at room temperature, and protected from light for 30 min. Blank samples (4 mL of DPPH + 200 μL of DMSO) were also prepared for each assay. The absorbance of the DPPH radical was then measured at 517 nm using a multimode microplate reader. Antioxidant activity was calculated according to the following equation: scavenging activity (%) = $[(Abs_{blank} - Abs_{sample}) / Abs_{blank}] \times 100\%$. All assays were performed in triplicate.

RESULTS AND DISCUSSION

Establishing a Molecular Nanovalve: Synthesis and Characterization. To gain a handle on the supramolecular complexation process, we first prepared an Azo@β-CD supramolecular complex (Figure 1A,B). The supramolecular complex was synthesized via a liquid−liquid diffusion method, specifically, by layering a methanolic solution of Azo on an aqueous solution of β-CD. Over a period of 14 d, the two layers diffused into one another to produce orange cubic crystals in a yield of 77%. The crystals were collected by suction filtration, washed with toluene until the filtrate was colorless, and finally washed with cold distilled water to ensure all of the β-CD starting material was removed (Supporting Information, Sections S1 and S2). A suitable single crystal of the Azo@β-CD supramolecular complex was analyzed by single-crystal X-ray diffraction (SCXRD), which revealed the supramolecular complex crystallized in the monoclinic $P2_1$ (No. 4) space group having lattice parameters of a = 15.3913(8), b = 31.8651(16), c = 31.0354(15) Å, α = 90, β = 102.325(3), and γ = 90° (Supporting Information, Table S1). From the single crystal structure, Azo was oriented perpendicularly to and centered inside the β-CD ring in a 1:1 ratio due to the formation of supramolecular interactions arising from the N atom of Azo with an H atom of β-CD. Although the Azo@β-CD supramolecular complex has been studied and reported in the literature,[25,26] this is the first report of its single crystal structure and, therefore, serves as an essential step toward establishing the concept of a molecular nanovalve in extended framework materials.

Further structural characterization of the Azo@β-CD supramolecular complex was performed by powder X-ray diffraction (PXRD) to establish bulk phase purity, ^{1}H−^{1}H homonuclear correlation nuclear magnetic resonance spectroscopy (^{1}H−^{1}H COSY NMR) to identify the supramolecular interactions, Fourier transform infrared spectroscopy (FT-IR) to further correlate the supramolecular interactions, thermal gravimetric analysis (TGA) to understand thermal stability, and microelemental analysis (EA) for chemical formulation. In the PXRD analysis of the bulk sample, the experimental diffraction pattern was in satisfactory agreement with the simulated diffraction pattern derived from the single crystal structure (Figure 1C). The ^{1}H−^{1}H COSY NMR spectrum showed that all internal correlations for Azo and β-CD were present as expected with the notable exception of one H atom: the axial H atom on C_4 of the D-glucose subunit chair conformation. This H atom was found to have a new correlation with the ortho-H atom to the azo moiety in Azo as a result of a new H-bond interaction between the aforementioned H atom in β-CD and the N atom(s) in Azo (Figure 1D). It is noted that this new correlation was absent in the ^{1}H−^{1}H COSY NMR spectrum acquired for a 1:1 w/w physical mixture of Azo and β-CD, respectively (Supporting Information, Figure S7). Indeed, these findings were in satisfactory agreement with interactions observed in the single crystal structure of the Azo@β-CD supramolecular complex. The TGA curve for the Azo@β-CD supramolecular complex displayed three distinct steps: step 1 occurred at 79 °C with an 8% weight loss, which was attributed to occluded solvent molecules (water and methanol); step 2 started at 164 °C with an 8% weight loss, which represented Azo decomplexation and thermal decomposition; and step 3 began at 273 °C with an 84% weight loss as a result of thermal decomposition of β-CD. Given the organic nature of the Azo@β-CD supramolecular complex, the sample was completely combusted leaving no residue. The TGA results were found to be in close agreement with the 1:1 Azo:β-CD ratio established by SCXRD in addition to the EA results that led to a chemical formula of $[(Azo)(\beta\text{-CD})(MeOH)_{0.25}]\cdot 4.25H_2O$ (Supporting Information, Figures S8−S10).

To establish the light stimuli-responsive opening of the molecular nanovalve via *trans*-to-*cis* isomerization of Azo and, therefore, decomplexation of the Azo@β-CD supramolecular complex, a heterogeneous cyclohexane mixture containing the Azo@β-CD supramolecular complex was irradiated with UV light (λ = 254 nm) for 19 h. As shown in Figure 1E, the concentration percentage of *trans*-Azo increased as a function of time upon irradiation, reaching a total of 25.7 ± 1.6%. Although appearing counterintuitive, this increase in the

https://doi.org/10.1021/acsami.4c01171
ACS Appl. Mater. Interfaces XXXX, XXX, XXX−XXX

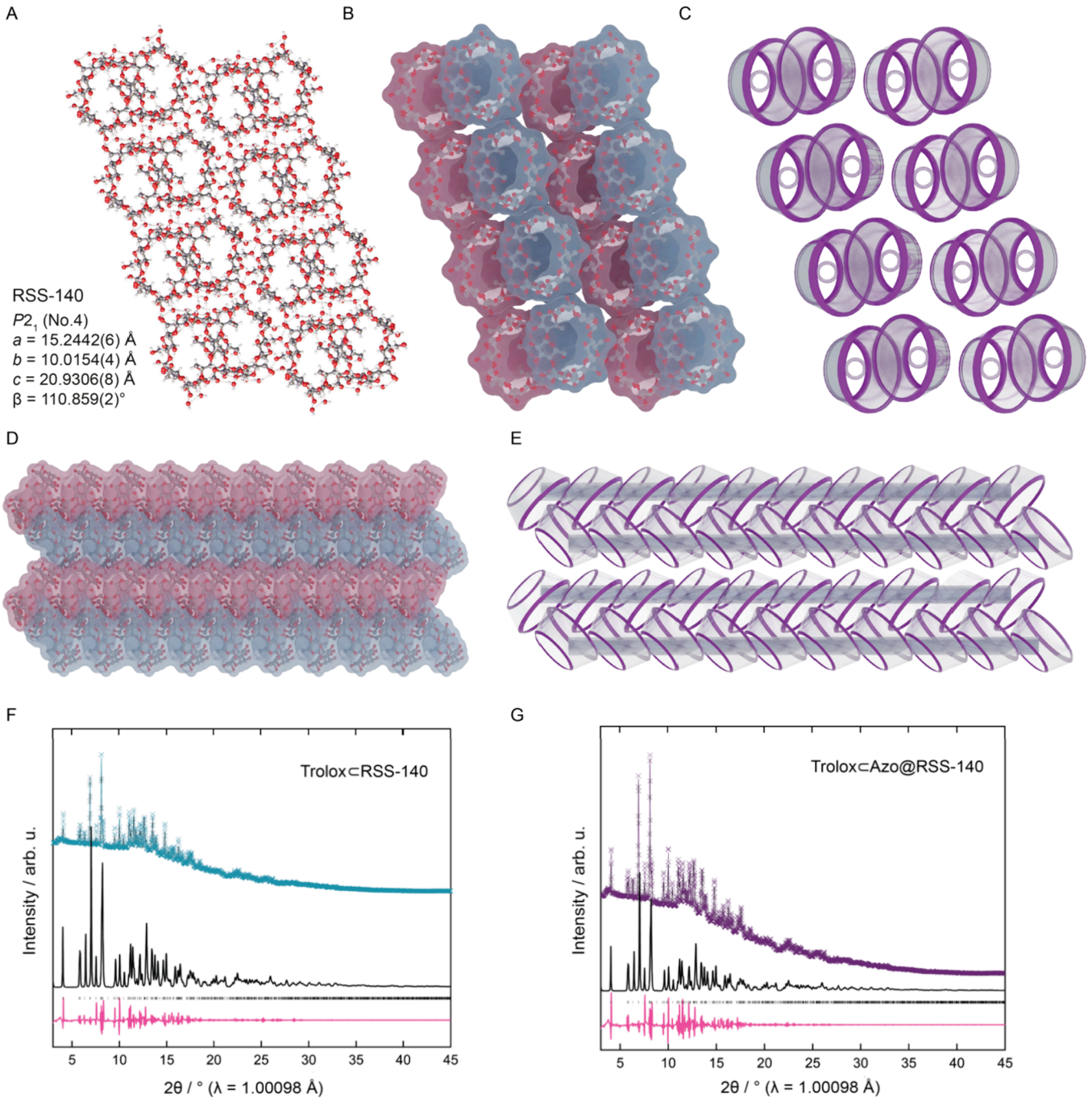

Figure 2. Synthesis, crystal structure, and structure characterization of RSS-140, Trolox⊂RSS-140, and Trolox⊂Azo@RSS-140. (A, B) Single crystal structure of RSS-140 with ball-and-stick and space-filling representations presented. (C) Illustration depicting the arrangement and orientation of the *β*-CD building units in RSS-140. (D, E) Packing of the *β*-CD building units in the single crystal structure of RSS-140 after rotating the structure shown in panel A +90° around the *y*-axis and −90° around the *x*-axis. (F, G) Synchrotron-light X-ray diffraction patterns of Trolox⊂RSS-140 and Trolox⊂Azo@RSS-140, respectively, showing the experimental (blue X symbols for Trolox⊂RSS-140 and purple X symbols for Trolox⊂Azo@RSS-140), Pawley refined (light gray), simulated RSS-140, and difference (pink) patterns. The Bragg positions are marked as black bars. Atom colors: C, gray; O, red; H, white. H-Bonds represented by red dashed lines.

concentration percentage of *trans*-Azo is to be expected as the *trans*-Azo in the Azo@*β*-CD supramolecular complex is first isomerized to *cis*-Azo, solubilized in the cyclohexane solvent, and then isomerized back to the more thermodynamically stable *trans* conformation. The decomplexation upon UV light irradiation was supported in the ^{1}H−^{1}H COSY NMR spectrum, whereby the characteristic chemical shifts for the supramolecular interactions observed in the Azo@*β*-CD supramolecular complex spectrum disappeared after 48 h of UV light irradiation (Figure 1F). Further support was provided by a control experiment in which the UV−vis spectrum was measured for the same mixture over 19 h in the absence of UV light irradiation. For this control experiment, no absorbance was detected for *trans*- or *cis*-Azo (Figure 1E).

After confirming the molecular nanovalve concept through the Azo@*β*-CD supramolecular complex, our attention turned

https://doi.org/10.1021/acsami.4c01171
ACS Appl. Mater. Interfaces XXXX, XXX, XXX−XXX

toward applying this concept to an extended framework material. Fortunately, β-CD has been used as an organic linker to construct a number of different metal−organic frameworks (MOFs) and our initial goal was to synthesize and apply the molecular nanovalve concept, via Azo, to the reported β-CD-MOF(K).[27−29] β-CD-MOF(K) was initially chosen as the target system given its nontoxicity and biocompatibility (i.e., K^+ ions used as a secondary building unit), ideal pore aperture size based on β-CD (9.4 × 8.4 Å) and its expected ability to load an antioxidant cargo molecule, Trolox, that has the appropriate molecular size (7.7 × 6.4 × 4.6 Å) and chemical functionalities (e.g., carboxylic acid and hydroxyl moieties) to fit through the pore aperture and be reasonably retained within the internal pores. Accordingly, colorless, rectangular single crystals were obtained in 84% yield by reacting β-CD and KOH in a 1:4 v/v solution of water and methanol in a Teflon-lined, stainless steel Parr autoclave at 140 °C for 3 days. SCXRD analysis revealed a structure that crystallized in the monoclinic $P2_1$ (No. 4) space group, with lattice parameters a = 15.2442(6), b = 10.0154(4), c = 20.9306(8) Å, α = 90, β = 110.859(2), and γ = 90°. At first glance, the structure appeared to be isostructural to the reported β-CD-MOF(K) (Cambridge Crystallographic Data Centre No. 2032038, CSD codes PULLUF, PULLUF01, and PULLUF02) with coincidental lattice parameters.[30−32] However, upon deeper analysis of the diffraction data, we determined that the K atoms could not be located during the structural refinement with only hydrogen-bonded water molecules being present to connect the packed β-CD building units; specifically, four different O atoms were clearly located and anisotropically refined, and seven electron density maximum positions were assigned to O atoms with partial occupancies, which were attributed to positionally disordered water molecules. One methanol solvent molecule was also clearly located and refined. We considered the possibility that some of these positions belong to K atoms being present with partial occupancies instead of water molecules. However, the corresponding refinements always led to significantly worse results, as indicated by higher residual values. Accordingly, via SCXRD analysis, we were able to absolutely confirm that, instead of the targeted β-CD-MOF(K), we realized a hydrogen-bonded organic framework (HOF), termed RSS-140, whose structure and pore metrics are nearly identical to that of β-CD-MOF(K) (Figures 2A−E), and is also consistent with previously determined β-CD hydrated structures.[33] The results of our crystallographic refinement demonstrate that, in RSS-140, each β-CD is hydrogen-bonded to nine neighboring β-CD building units (16 points of extension) via either the β-CD's hydroxyl groups and/or through interstitial water molecules (Supporting Information, Figures S21−S25).

Three systems were then prepared for further study: (i) RSS-140 as the parent, pristine HOF; (ii) Trolox⊂RSS-140 as the control HOF having Trolox loaded within the pores but without the nanovalve; and (iii) Trolox⊂Azo@RSS-140 as the target system with Trolox loaded and held within RSS-140 by an Azo nanovalve. Trolox⊂RSS-140 and Trolox⊂Azo@RSS-140 were synthesized following the same procedure as before, with the notable exceptions of adding Trolox and Trolox/Azo to the reaction mixtures, respectively. The syntheses of Trolox⊂RSS-140 and Trolox⊂Azo@RSS-140 afforded colorless and pale-yellow rectangular crystals in 80 and 79% yields, respectively (Supporting Information, Section S2).

SCXRD analysis of Trolox⊂RSS-140 afforded comparable results with similar positions for adsorbed water molecules, demonstrating that the same arrangement of β-CD building units occurs even in the presence of Trolox (Supporting Information, Table S5). The exact position of the Trolox molecules could not be determined from this refinement, most likely as a result of a low loading amount. Furthermore, SCXRD analysis for Trolox⊂Azo@RSS-140 further showed no change in the arrangement of β-CD building units; however, a large amount of residual electron density was observed in the voids of the hydrogen-bonded β-CD building units (Supporting Information, Table S6). Unsuccessful attempts were made to describe this residual electron density according to the presence of Trolox and Azo molecules. This is not surprising considering that this electron density represents an average for the crystal, and the Trolox and Azo molecules are not expected to be periodically present inside each β-CD molecule, but rather randomly distributed. Nevertheless, by using a solvent mask technique, it was found that this electron density inside the cavities of the β-CDs corresponds to 116 e^- per unit cell, which is consistent with the presence of one Trolox and one Azo every other unit cell (i.e., 1 Trolox +1 Azo = 230 e^-).

A full pattern profile refinement (Pawley) with use of synchrotron collected data (λ = 1.00098 Å) was carried out for Trolox⊂RSS-140 and Trolox⊂Azo@RSS-140 resulting in excellent agreements and demonstrating that the bulk sample consists of pure crystalline phase of RSS-140 with no other byproduct phase (e.g., β-CD-MOF(K)) nor crystalline form for Trolox or Azo being present (Figures 2F,G). Digestion ^{1}H NMR spectroscopy in deuterated dimethyl sulfoxide (DMSO-d_6) was employed to quantify Trolox loading and Azo complexation. When comparing the ^{1}H NMR spectrum of RSS-140 with the spectrum of β-CD alone, the hydroxyl H atoms of β-CD (chemical shifts = 4.44, 5.67, and 5.71 ppm) remained in the RSS-140 spectrum, which confirmed the nonbonding between β-CD and K^+ ions. In the Trolox⊂RSS-140 ^{1}H NMR spectrum, the expected chemical shifts were present in addition to nine new chemical shifts that were attributed to Trolox. Integration of these new chemical shifts with respect to the chemical shifts assigned to RSS-140 led to a calculated 1% w/w loading capacity. For the ^{1}H NMR spectrum of Trolox⊂Azo@RSS-140, the expected chemical shifts characteristic of Trolox⊂RSS-140 were observed alongside three new chemical shifts ascribed to Azòs aromatic protons. From integration, the loading of Trolox and the presence of Azo were quantified as 1.65 and 0.56% w/w, respectively (Supporting Information, Figures S29−S33). It is noted that these loading amounts were further substantiated by elemental microanalysis (Supporting Information, Section S2). The higher loading of Trolox in Trolox⊂Azo@RSS-140 occurs due to the Azo nanovalve locking the Trolox within the pores of the HOF. The TGA curves for RSS-140, Trolox⊂RSS-140, and Trolox⊂Azo@RSS-140 exhibit similar thermal decomposition profiles; specifically, all are thermally stable up to ca. 290 °C (Supporting Information, Figures S34−S37).

Prior to studying the kinetics of the nanovalve opening and the subsequent release of Trolox, solvent stability tests were performed. In a typical experiment, Trolox⊂Azo@RSS-140 was immersed in hexane, cyclohexane, dichloromethane, or water for 24 h, at which point the HOF was removed from the solvent and air-dried before PXRD analysis. It is noted that the Trolox⊂Azo@RSS-140 retained its crystalline nature for hexane and cyclohexane, became amorphous in dichloro-

https://doi.org/10.1021/acsami.4c01171
ACS Appl. Mater. Interfaces XXXX, XXX, XXX−XXX

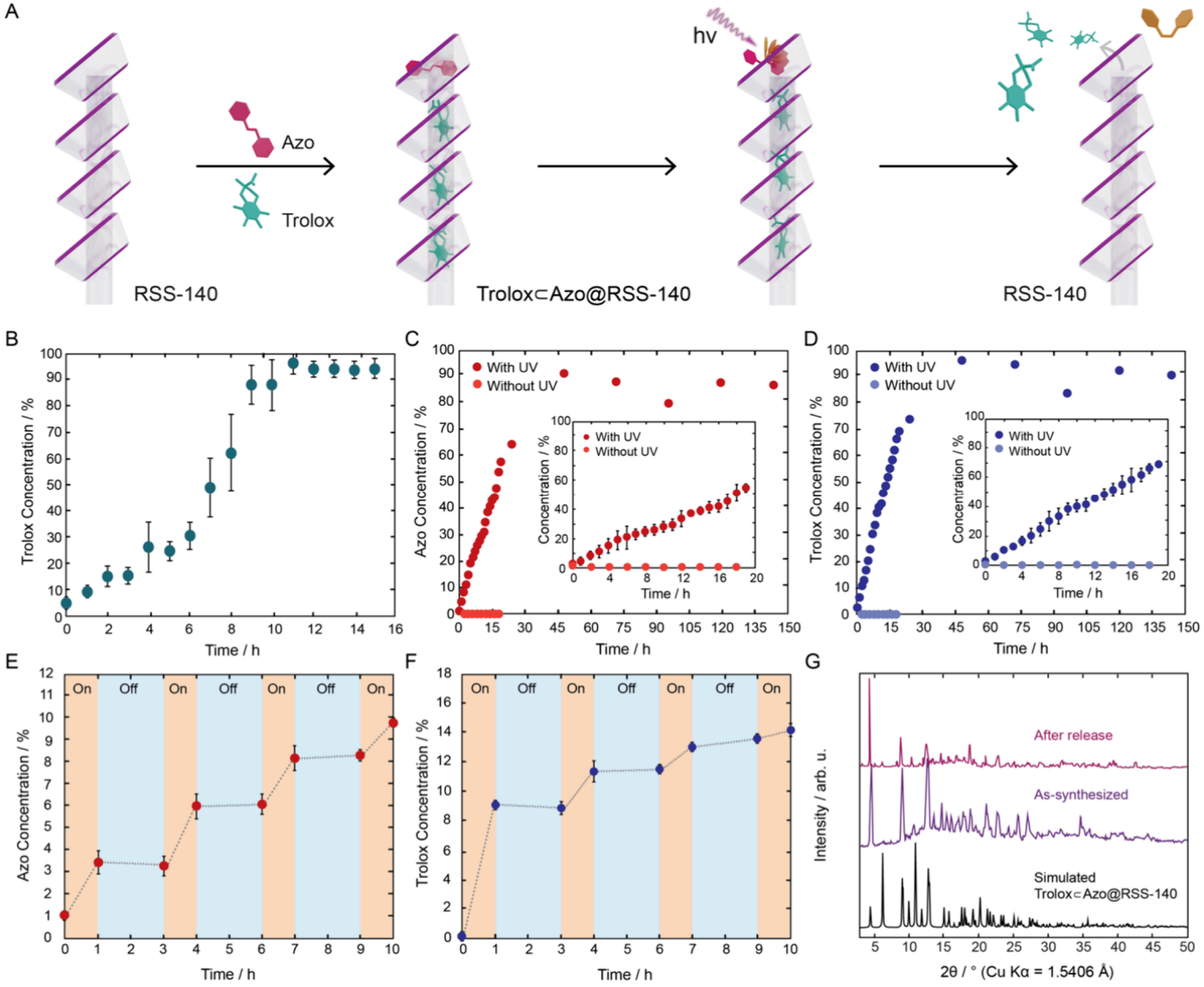

Figure 3. Molecular nanovalve in action: light-stimulated opening of the RSS-140. (A) Illustration depicting the formation of Trolox⊂Azo@RSS-140 and subsequent release of Trolox upon the light-stimulated opening of RSS-140. (B) Release of Trolox from Trolox⊂RSS-140 at 25 °C monitored at λ = 290 nm. (C) Full release of Azo from Trolox⊂Azo@RSS-140 at 25 °C monitored at λ = 320 nm. Inset shows the initial release up to 19 h. (D) Full release of Trolox from Trolox⊂Azo@RSS-140 at 25 °C monitored at λ = 290 nm. Inset shows the initial release up to 19 h. (E) On−off release of Azo from Trolox⊂Azo@RSS-140 at 25 °C monitored at λ = 320 nm. (F) On−off release of Trolox from Trolox⊂Azo@RSS-140 at 25 °C and monitored at λ = 290 nm. (G) Comparison of the simulated PXRD pattern of RSS-140 (black) with the experimental diffraction patterns of as-synthesized Trolox⊂Azo@RSS-140 (purple) and Trolox⊂Azo@RSS-140 (pink) after the full release experiments, which demonstrates structural stability throughout the measurements. Error bars depict standard deviation (n = 3).

methane, and completely dissolved in water (Supporting Information, Figure S38). The fact that Trolox⊂Azo@RSS-140 is stable in cyclohexane is important for the following reasons: (i) Trolox and Azo alone are soluble in cyclohexane, which allows for monitoring their release from RSS-140 by UV−vis spectroscopy; (ii) the Azo@β-CD supramolecular complex is insoluble and shows no sign of decomplexation in cyclohexane; and (iii) pure cyclohexane is UV inactive. Finally, a long-term stability study was conducted for Trolox⊂Azo@RSS-140, from which the PXRD pattern remained relatively unchanged after 6 and 12 m of storing Trolox⊂Azo@RSS-140 in a dry, dark environment (Supporting Information, Figure S39).

Trolox Release Kinetics for Light-Stimulated Opening of RSS-140 Equipped with a Molecular Nanovalve. To establish the baseline release kinetics of Trolox from RSS-140, we placed Trolox⊂RSS-140 in cyclohexane and took hourly UV−vis measurements until all of the Trolox was observed to have been released (Figure 3). From these measurements, it was very clear that Trolox leached out of the pores of RSS-140 quickly and uncontrollably, as highlighted by a 14 ± 3.8% increase in Trolox concentration in the supernatant within 2 h. The leaching continued as a function of time reaching a total of 62 ± 15% Trolox concentration after 8 h and the Trolox concentration reached full saturation (96 ± 4.5%) in the supernatant by 11 h (Figure 3B). The release profile for Trolox⊂RSS-140 can be described as sigmoidal, and a reasonable correlation constant was calculated when fitting this release profile to a concentration-dependent first order kinetic model (Supporting Information, Figure S42). PXRD analysis on the RSS-140 post-Trolox leaching showed that the crystallinity and structure were retained (Supporting Information, Figure S43).

https://doi.org/10.1021/acsami.4c01171
ACS Appl. Mater. Interfaces XXXX, XXX, XXX−XXX

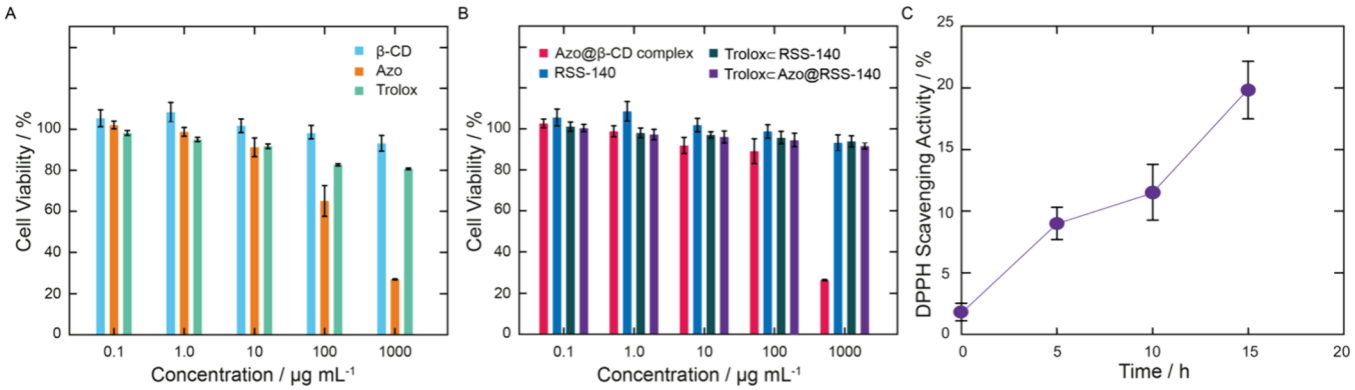

Figure 4. *In vitro* cytotoxicity and antioxidant activity assays. Cytotoxicity was evaluated through a cell viability assay after treating human dermal fibroblast (HDF) cells with varying concentrations (0.1−1000 μg mL^{-1}) (A) β-CD (light blue), Azo (orange), and Trolox (light green) and (B) Azo@β-CD (pink), RSS-140 (blue), Trolox⊂RSS-140 (dark green), and Trolox⊂Azo@RSS-140 (purple) for 72 h. Shown are HDF cell viability percentages as a function of concentration. Error bars depict standard deviation (n = 5). (C) Antioxidant activity was assessed via an *in vitro* 2,2-diphenyl-1-picrylhydrazyl (DPPH) radical scavenging assay after exposing Trolox⊂Azo@RSS-140 to UV light (λ = 254 nm) as a function of time (0, 5, 10, and 15 h). Error bars depict standard deviation (n = 3).

Our attention then turned to assessing whether Trolox⊂Azo@RSS-140 could effectively control the release of Trolox. In a similar experimental setup, Trolox⊂Azo@RSS-140 was placed in cyclohexane without UV irradiation and hourly UV−vis measurements were taken for aliquots of the supernatant. Remarkably, neither Trolox nor Azo was observed in the supernatant even after 3 and 6 m (Supporting Information, Figures S46 and S47). This finding is an incredibly important step toward demonstrating the effectiveness of the nanovalve locking the Trolox cargo inside of RSS-140. To controllably release Trolox, Trolox⊂Azo@RSS-140 in cyclohexane was continuously irradiated with UV light (λ = 254 nm) for 144 h. For the first 19 h, hourly UV−vis measurements were performed to track the Azo decomplexation and subsequent Trolox release. As depicted in Figure 3C,D, a nearly linear, slow, and controlled release of both Azo and Trolox was observed. This behavior was in line with expectations as the Azo under UV light isomerizes and, therefore, decomplexes before allowing Trolox to release from the internal pores. Opening of the Azo nanovalve and releasing of the Trolox under UV light continues to completion at 48 h. The Azo and Trolox release profiles were linear and were satisfactorily fitted by a concentration-independent zero order kinetic model (Supporting Information, Figures S48 and S49). To demonstrate a higher degree of control over opening the nanovalve, we carried out a third experiment whereby the Trolox⊂Azo@RSS-140 was alternatively exposed to UV light for 1 h and then kept in the dark for 2 h; an on−off cycle that was repeated three times. Accordingly, during the UV-on 1 h phases of each on−off cycle, the Azo and Trolox release profiles were as expected. On the other hand, during the UV-off, dark 2 h phases, neither Azo nor Trolox were released from the Trolox⊂Azo@RSS-140 (Figure 3E,F). After the culmination of each of these experiments, PXRD analysis confirmed that the structure of RSS-140 was maintained (Figure 3G).

***In Vitro* Cytotoxicity and Antioxidant Activity Assays.** Given the successful demonstration of the molecular nanovalve concept in Trolox⊂Azo@RSS-140, our attention turned to demonstrating its practical applicability. It is noted that Trolox was specifically chosen as the cargo because of its ability to scavenge free radicals and prevent oxidative damage in human dermal fibroblast (HDF) cells upon exposure to UV light.[34−36] The beauty of the Trolox⊂Azo@RSS-140 design is that it requires UV light activation, an environment, and time when protection for HDF cells against the harmful effects of UV light is needed most and can be sustainably provided by released Trolox.

Accordingly, HDF cells were incubated with varying concentrations (0, 0.1, 1, 10, 100, and 1000 μg mL^{-1}) of Azo, Trolox, β-CD, Azo@β-CD supramolecular complex, RSS-140, and Trolox⊂RSS-140 as controls in addition to the full system of Trolox⊂Azo@RSS-140 for 72 h. The cytotoxicity of each was then assessed via a resazurin assay, with Figure 4A,B illustrating the cell viability percentage after 72 h of treatment. From these assays, the cytotoxicity of Azo and Azo@β-CD supramolecular complex was observed to be concentration-dependent, at lower concentrations up to 10 μg mL^{-1}, >90% of the HDF cells were viable, but at the high concentration of 1000 μg mL^{-1}, only ca. 25% of the HDF cells were found to be viable. The cytotoxicities of β-CD, RSS-140, and Trolox⊂RSS-140 were observed to be concentration-independent with cell viabilities >90% being retained even at 1000 μg mL^{-1}. Finally, Trolox⊂Azo@RSS-140 exhibited concentration-independent low cytotoxicity given that >90% of the HDF cells remained viable at high concentrations of 1000 μg mL^{-1}. Although Azo alone has a certain level of cytotoxicity, its concentration in Trolox⊂Azo@RSS-140 is low and, therefore, does not negatively impact the cytotoxicity of the full system. When taken together, these findings are important as they effectively demonstrate the safety and nontoxicity of Trolox⊂Azo@RSS-140 when applied to human skin.

Although it is an important step forward to establish the safety of Trolox⊂Azo@RSS-140, it is imperative to also demonstrate its effectiveness in serving as a stimuli-responsive antioxidant delivery system. Accordingly, an *in vitro* 2,2-diphenyl-1-picrylhydrazyl (DPPH) radical scavenging assay was performed using Trolox⊂Azo@RSS-140. In this experiment, Trolox⊂Azo@RSS-140 was exposed to UV light (λ = 254 nm) as a function of time (0, 5, 10, and 15 h) to open the molecular nanovalve and release the Trolox cargo. As is shown in Figure 4C, two important findings were observed: (i) as expected, Trolox⊂Azo@RSS-140 exhibited increasing antioxidant activity as a function of time, and (ii) the antioxidant properties of Trolox were not altered during the synthesis and

https://doi.org/10.1021/acsami.4c01171
ACS Appl. Mater. Interfaces XXXX, XXX, XXX−XXX

preparation of Trolox⊂Azo@RSS-140 nor due to exposure of UV light. To ensure that the antioxidant activity was solely derived from Trolox, a control experiment was then performed by separately dissolving RSS-140 and the Azo@β-CD supramolecular complex in DMSO and DPPH solution. Indeed, neither RSS-140 nor the Azo@β-CD supramolecular complex exhibited any antioxidant activity.

CONCLUSIONS

The work reported herein yields a conceptual advance with respect to equipping a biocompatible, extended, solid-state HOF structure (e.g., RSS-140) with a stimuli-responsive molecular nanovalve (e.g., Azo@β-CD). The molecular nanovalve concept is important in that it enables a given HOF to have built-in controllable release capabilities for delivering active ingredients. Specifically, by exploiting the chemistry of supramolecular complexation, we were able to use the pore windows of RSS-140 as the opening for installing an Azo molecule that serves as the molecular nanovalve. This approach is distinctly different from the limited number of related reports as our system is built from a biologically friendly building unit (i.e., β-CD), does not require multistep building block synthesis, and avoids mass transport issues associated with having an azo moiety attached to the backbone of or be positioned within the HOF.[13,15,37] Upon loading RSS-140 with an active ingredient (i.e., Trolox), active leaching was witnessed, which was completely halted when the molecular nanovalve was installed and the opening was closed. Indeed, it was only when the Trolox⊂Azo@RSS-140 was exposed to light of a specific wavelength that the nanovalve could open to allow subsequent release of the Trolox to be realized. Finally, preliminary *in vitro* cellular studies (i.e., cytotoxicity and antioxidant ability) provide early indication of the safety and nontoxicity of Trolox⊂Azo@RSS-140 to human dermal fibroblast cells as well as its effectiveness in delivering on-demand antioxidant properties.

We note that according to scanning electron microscopy (SEM) imaging, the relative particle size of Trolox⊂Azo@RSS-140 is on the order of 100 μm (Supporting Information, Figure S58). This size is ideal for use in topical *in vivo* and/or clinical experiments/applications, as the particles will not be able to pass through the skin, thereby significantly minimizing any unexpected off-target effects. Looking forward, our lab is currently undertaking formulation studies using suitable, water-insoluble surfactants that Trolox⊂Azo@RSS-140 remains stable in to demonstrate the successful translation of the molecular nanovalve concept in Trolox⊂Azo@RSS-140 to a cosmetic skin-care product that provides effective remediation of UV damage to skin. Indeed, this is a promising approach, as in preliminary results Trolox⊂Azo@RSS-140 exhibits structural stability after immersion in Capryol 90 for 1 week (Supporting Information, Figure S59). Finally, as the field of supramolecular chemistry is rich with similar systems and many such systems can be used as building blocks to construct HOFs, MOFs, or even porous polymers, we envision the molecular nanovalve concept to be applied widely for controllably delivering cargo for many different applications.

ASSOCIATED CONTENT

Data Availability Statement

These data are provided free of charge by the joint Cambridge Crystallographic Data Centre and Fachinformationszentrum Karlsruhe Access Structures service.

Supporting Information

The Supporting Information is available free of charge at https://pubs.acs.org/doi/10.1021/acsami.4c01171.

Experimental details, materials, and methods, single crystal and powder X-ray diffraction data, nuclear magnetic resonance spectra, Fourier transform infrared spectra, optical and scanning electron microscopy analysis, Trolox and Azo release measurements, *in vitro* cellular experiments, and crystallographic and structure refinement data of deposition nos. 2285699 (RSS-140), 2285700 (Trolox⊂RSS-140), 2285701 (Trolox⊂Azo@RSS-140), and 2285816 (Azo@β-CD supramolecular complex) (PDF)

Crystallographic data of Azo@β-CD supramolecular complex (CIF)

Crystallographic data of RSS-140 (CIF)

Crystallographic data of Trolox⊂RSS-140 (CIF)

Crystallographic data of Trolox⊂Azo@RSS-140 (CIF)

AUTHOR INFORMATION

Corresponding Author

Kyle E. Cordova − *Integrated Materials Systems Research Unit, Advanced Research Centre, Royal Scientific Society, Amman 11941, Jordan;* orcid.org/0000-0002-4988-0497; Email: cordovak10@gmail.com

Authors

Sara A. Ghazal − *Integrated Materials Systems Research Unit, Advanced Research Centre, Royal Scientific Society, Amman 11941, Jordan*

Sarah W. Tabbalat − *Integrated Materials Systems Research Unit, Advanced Research Centre, Royal Scientific Society, Amman 11941, Jordan*

Felipe Gándara − *Materials Science Institute of Madrid, Consejo Superior de Investigaciones Cientificas, Madrid 28049, Spain;* orcid.org/0000-0002-1671-6260

Ala'a Al-Ghourani − *Integrated Materials Systems Research Unit, Advanced Research Centre, Royal Scientific Society, Amman 11941, Jordan*

Samah M. Abusulieh − *Faculty of Pharmacy, Al-Zaytoonah University of Jordan, Amman 11733, Jordan*

Mahmoud Abdellatief − *Synchrotron-light for Experimental Science and Applications in the Middle East (SESAME), Allan 19252, Jordan*

Suhair Sunoqrot − *Faculty of Pharmacy, Al-Zaytoonah University of Jordan, Amman 11733, Jordan*

Complete contact information is available at: https://pubs.acs.org/10.1021/acsami.4c01171

Funding

Financial support was provided by the Newton-Khalidi Fund and the Royal Academy of Engineering's Transforming Systems through Partnership program (No. TSP2021/100001), Al-Zaytoonah University of Jordan (No. 14/08/2021−2022), in addition to the Royal Scientific Society.

Notes

The authors declare the following competing financial interest(s): A patent has been filed: Royal Scientific Society (patent application), K.E.C., S.A.G. and S.W.T. (inventors), PCT application no. US63/536,439 with a priority date of September 4, 2023. The authors declare no other competing interests.

https://doi.org/10.1021/acsami.4c01171
ACS Appl. Mater. Interfaces XXXX, XXX, XXX−XXX

■ ACKNOWLEDGMENTS

The authors are grateful for the advice, guidance, and helpful discussions provided by Prof. Stuart A. Jones (King's College London), Prof. Khuloud T. Al-Jamal (King's College London), Dr. Bassem Al-Maythalony (Royal Scientific Society), and Prof. Muayad Esaifan (University of Petra). The authors wish to thank Dr. Diya Al Safadi (Royal Scientific Society) for access to instrumentation. K.E.C. and S.A.G. extend their appreciation to Ms. Rada Abaza (Royal Scientific Society), Mr. Obieda S. Mudraj (Royal Scientific Society), Mr. Osama Abu Hasan, and Ms. Ashley M. Osborn for their contributions to the project.

■ REFERENCES

(1) Balzani, V.; Credi, A.; Raymo, F. M.; Stoddart, J. F. Artificial Molecular Machines. *Angew. Chem., Int. Ed.* **2000**, *39*, 3348−3391.
(2) Browne, W. R.; Feringa, B. L. Making Molecular Machines Work. *Nat. Nanotechnol.* **2006**, *1*, 25−35.
(3) Aprahamian, I. The Future of Molecular Machines. *ACS Cent. Sci.* **2020**, *6*, 347−358.
(4) Kay, E. R.; Leigh, D. A. Rise of the Molecular Machines. *Angew. Chem., Int. Ed.* **2015**, *54*, 10080−10088.
(5) Coskun, A.; Banaszak, M.; Astumian, R. D.; Stoddart, J. F.; Grzybowski, B. A. Great Expectations: can Artificial Molecular Machines Deliver on their Promise? *Chem. Soc. Rev.* **2012**, *41*, 19−30.
(6) Kocer, A.; Walko, M.; Meijberg, W.; Feringa, B. L. A Light-actuated Nanovalve Derived from a Channel Protein. *Science* **2005**, *309*, 755−758.
(7) Heard, A. W.; Goldup, S. M. Simplicity in the Design, Operation, and Applications of Mechanically Interlocked Molecular Machines. *ACS Cent. Sci.* **2020**, *6*, 117−128.
(8) Ferris, D. P.; Zhao, Y.-L.; Khashab, N. M.; Khatib, H. A.; Stoddart, J. F.; Zink, J. I. Light-operated Mechanized Nanoparticles. *J. Am. Chem. Soc.* **2009**, *131*, 1686−1688.
(9) Hernandez, R.; Tseng, H.-R.; Wong, J. W.; Stoddart, J. F.; Zink, J. I. An Operational Supramolecular Nanovalve. *J. Am. Chem. Soc.* **2004**, *126*, 3370−3371.
(10) Nguyen, T. D.; Leung, K. C.-F.; Liong, M.; Pentecost, C. D.; Stoddart, J. F.; Zink, J. I. Construction of a pH-Driven Supramolecular Nanovalve. *Org. Lett.* **2006**, *8*, 3363−3366.
(11) Nguyen, T. D.; Tseng, H.-R.; Celestre, P. C.; Flood, A. H.; Liu, Y.; Stoddart, J. F.; Zink, J. I. A Reversible Molecular Valve. *Proc. Natl. Acad. Sci. U. S. A.* **2005**, *102*, 10029−10034.
(12) Nguyen, T. D.; Leung, K. C.-F.; Liong, M.; Liu, Y.; Stoddart, J. F.; Zink, J. I. Versatile Supramolecular Nanovalves Reconfigured for Light Activation. *Adv. Funct. Mater.* **2007**, *17*, 2101−2110.
(13) Meng, X.; Gui, B.; Yuan, D.; Zeller, M.; Wang, C. Mechanized Azobenzene-functionalized Zirconium Metal-Organic Framework for On-command Cargo Release. *Sci. Adv.* **2016**, *2*, No. e1600480.
(14) Deng, H.; Olson, M. A.; Stoddart, J. F.; Yaghi, O. M. Robust Dynamics. *Nat. Chem.* **2010**, *2*, 439−443.
(15) Tan, L.-L.; Song, N.; Zhang, S. X.-A.; Li, H.; Wang, B.; Yang, Y.-W. Ca^{2+}, pH, and Thermo Triple-responsive Mechanized Zr-based MOFs for On-command Drug Release in Bone Diseases. *J. Mater. Chem. B* **2016**, *4*, 135−140.
(16) Angelos, S.; Khashab, N. M.; Yang, Y.-W.; Trabolsi, A.; Khatib, H. A.; Stoddart, J. F.; Zink, J. I. pH Clock-Operated Mechanized Nanoparticles. *J. Am. Chem. Soc.* **2009**, *131* (36), 12912−12914.
(17) Ambrogio, M. W.; Pecorelli, T. A.; Patel, K.; Khashab, N. M.; Trabolsi, A.; Khatib, H. A.; Botros, Y. Y.; Zink, J. I.; Stoddart, J. F. Snap-Top Nanocarriers. *Org. Lett.* **2010**, *12* (15), 3304−3307.
(18) Furukawa, H.; Cordova, K. E.; O'Keeffe, M.; Yaghi, O. M. The Chemistry and Applications of Metal-Organic Frameworks. *Science* **2013**, *341*, No. 1230444.
(19) Diercks, C. S.; Liu, Y.; Cordova, K. E.; Yaghi, O. M. The Role of Reticular Chemistry in the Design of CO_2 Reduction Catalysts. *Nat. Mater.* **2018**, *16*, 301−307.
(20) Zha, X.; Li, X.; Al-Omari, A. A.; Liu, S.; Liang, C.; Al-Ghourani, A.; Abdellatief, M.; Yang, J.; Nguyen, H. L.; Al-Maythalony, B.; Shi, Z.; Cordova, K. E.; Zhang, Y. Zeolite NPO-Type Azolate Frameworks. *Angew. Chem., Int. Ed.* **2022**, *134*, No. e202207467.
(21) Xu, T.; Zhou, B.; Tao, Y.; Shi, Z.; Jiang, W.; Abdellatief, M.; Cordova, K. E.; Zhang, Y. B. Functionality-Induced Locking of Zeolitic Imidazolate Frameworks. *Chem. Mater.* **2023**, *35*, 490−498.
(22) Yuan, S.; Zou, L.; Qin, J. S.; Li, J.; Huang, L.; Feng, L.; Wang, X.; Bosch, M.; Alsalme, A.; Cagin, T.; Zhou, H. C. Construction of Hierarchically Porous Metal-Organic Frameworks through Linker Labilization. *Nat. Commun.* **2017**, *8*, 15356.
(23) Deng, H.; Grunder, S.; Cordova, K. E.; Valente, C.; Furukawa, H.; Hmadeh, M.; Gandara, F.; Whalley, A. C.; Liu, Z.; Asahina, S.; Kazumori, H.; O'Keeffe, M.; Terasaki, O.; Stoddart, J. F.; Yaghi, O. M. Large-pore Apertures in a Series of Metal-Organic Frameworks. *Science* **2012**, *336*, 1018−1023.
(24) Brown, J. W.; Henderson, B. L.; Kiesz, M. D.; Whalley, A. C.; Morris, W.; Grunder, S.; Deng, H.; Furukawa, H.; Zink, J. I.; Stoddart, J. F.; Yaghi, O. M. Photophysical Pore Control in an Azobenzene-containing Metal-Organic Framework. *Chem. Sci.* **2013**, *4*, 2858−2864.
(25) Wang, D.; Zhao, W.; Wei, Q.; Zhao, C.; Zheng, Y. Photoswitchable Azobenzene/cyclodextrin Host-guest Complexes: From UV-to Visible/Near-IR-Light-Responsive Systems. *ChemPhotoChem.* **2018**, *2*, 403−415.
(26) Harada, A.; Takashima, Y.; Nakahata, M. Supramolecular Polymeric Materials via Cyclodextrin-Guest Interactions. *Acc. Chem. Res.* **2014**, *47*, 2128−2140.
(27) Dummert, S. V.; Saini, H.; Hussain, M. Z.; Yadava, K.; Jayaramulu, K. K.; Casini, A.; Fischer, R. A. Cyclodextrin Metal-Organic Frameworks and Derivatives: Recent Developments and Applications. *Chem. Soc. Rev.* **2022**, *51*, 5175−5213.
(28) Smaldone, R. A.; Forgan, R. S.; Furukawa, H.; Gassensmith, J. J.; Slawin, A. M. Z.; Yaghi, O. M.; Stoddart, J. F. Metal-Organic Frameworks from Edible Nature Products. *Angew. Chem., Int. Ed.* **2010**, *49*, 8630−8634.
(29) Roy, I.; Stoddart, J. F. Cyclodextrin Metal-Organic Frameworks and their Applications. *Acc. Chem. Res.* **2021**, *54*, 1440−1453.
(30) Sha, J.-Q.; Wu, L.-H.; Li, S.-X.; Yang, X.-N.; Zhang, Y.; Zhang, Q.-N.; Zhu, P.-P. Synthesis and Structure of New Carbohydrate Metal−Organic Frameworks and Inclusion Complexes. *J. Mol. Struct.* **2015**, *1101*, 14−20.
(31) Yang, A.; Liu, H.; Li, Z.; Li, L.; Li, W.; Liu, K. Green Synthesis of β-Cyclodextrin Metal−Organic Frameworks and the Adsorption of Quercetin and Emodin. *Polyhedron* **2019**, *159*, 116−126.
(32) Jiang, W.; Liu, H.; Liao, Q.; Tang, T.; Liu, J.; Liu, Z.; Xie, L.; Yan, J. Preparation of Two Metal-Organic Frameworks (K-β-CD-MOFs and Cs-β-CD-MOFs) and the Adsorption Research of Myricetin. *Polyhedron* **2021**, *196*, No. 114983.
(33) Lindner, K.; Saenger, W. β-Cyclodextrin Dodecahydrate: Crowding of Water Molecules within a Hydrophobic Cavity. *Angew. Chem., Int. Ed.* **1978**, *17*, 694−695.
(34) Alberto, M. E.; Russo, N.; Grand, A.; Galano, A. A Physicochemical Examination of the Free Radical Scavenging Activity of Trolox: Mechanism, Kinetics and Influence of the Environment. *Phys. Chem. Chem. Phys.* **2013**, *15*, 4642−4650.
(35) Forrest, V. J.; Kang, Y.-H.; McClain, D. E.; Robinson, D. H.; Ramakrishnan, N. Oxidative Stress-induced Apoptosis Prevented by Trolox. *Free Rad. Bio. Med.* **1994**, *16*, 675−684.
(36) van den Berg, R.; Haenen, G. R. M. M.; van den Berg, H. H.; Bast, A. Applicability of an Improved Trolox Equivalent Antioxidant Capacity (TEAC) Assay for Evaluation of Antioxidant Capacity Measurements of Mixtures. *Food Chem.* **1999**, *66*, 511−517.
(37) Wu, M.; Gao, J.; Wang, F.; Yang, J.; Song, N.; Jin, X.; Mi, P.; Tian, J.; Luo, J.; Liang, F.; Yang, Y. Multistimuli Responsive Core-shell Nanoplatform Constructed from Fe_2O_4@MOF Equipped with Pillar[6]arene Nanovalves. *Small* **2018**, *14*, No. 1704440.

https://doi.org/10.1021/acsami.4c01171
ACS Appl. Mater. Interfaces XXXX, XXX, XXX−XXX